

## Attosecond-precision balanced timing detector with a single photodiode

TONG WANG,<sup>1</sup> MINGZHE LI,<sup>1</sup> YI ZHANG,<sup>1</sup> AND MING XIN<sup>1,2,\*</sup> 

<sup>1</sup>School of Electrical and Information Engineering, Tianjin University, Tianjin 300072, China

<sup>2</sup>Tianjin Key Laboratory of Brain-Inspired Intelligence Technology, Tianjin 300072, China

\*xinm@tju.edu.cn

Received 11 September 2023; accepted 12 September 2023; posted 15 September 2023; published 29 September 2023

We experimentally demonstrate a novel and practical timing detector based on a double-pass acousto-optic frequency shifter. With time and frequency multiplexing, for the first time to our knowledge, a balanced detection is realized using only a single photodiode, which greatly decreases the excess electronic noise during photodetection. With a total input optical power of 1.4 mW (0.35 mW per pulse train), an almost shot-noise-limited detection floor of 28.3 zs/√Hz is achieved, and the timing jitter integrated from 1 kHz to 1 MHz is reduced from 99.0 as (without eliminating the photodetector electronic noise) to only 30.4 as. Even with an input power of 50 μW per pulse train, 221.4 zs/√Hz detection floor and 268.0 as integrated timing jitter at [1 kHz and 1 MHz] are still maintained. This timing detector provides a powerful tool for high-precision metrology, ultra-long-distance ranging, and large-scale timing synchronization. © 2023 Optica Publishing Group

<https://doi.org/10.1364/OL.505656>

Timing metrology benefits greatly from recent advances in femtosecond mode-locked lasers and frequency combs with intrinsically a low timing jitter (<<1 fs) at a high-frequency range. Consequently, a high-precision timing detector based on mode-locked lasers has become an indispensable component in many advanced scientific applications, such as remote laser/microwave synchronization [1–3] and pump–probe measurements [4,5] in x ray free electron lasers (XFEL) [6,7], strain sensing [8], optical clocks [9], waveform synthesis [10], multi-telescope arrays [11], time-of-flight sensing [12,13], and soliton characterization [14,15].

In the past two decades, several approaches leveraging mode-locked lasers have been proposed to attain exceptional timing precision. The conventional direct timing characterization method is commonly achieved by converting the laser pulse to the RF signal with a high-speed photodiode (PD), yet the timing resolution is strictly limited by the amplitude modulation to phase modulation (AM-to-PM) transformation noise induced during photodetection. The balanced optical cross-correlator (BOC) technique [16] was then developed to circumvent this issue, and its intrinsic immunity to AM-to-PM noise firstly enabled the measurement precision to the attosecond level. To date, the BOC method continues to reign as the preeminent and ubiquitous timing detection technique worldwide

[1–3,10,14,15] with a resolution up to 122 ys/√Hz after data processing [17]. Nonetheless, the timing resolution of BOC is severely restricted by the low sum-frequency generation efficiency in the nonlinear crystal, making it only work efficiently at >10 mW input power levels. To break the power barrier of BOC, several linear-optics-based timing detection schemes have been reported [18–20]. With the balanced low-power timing detector (BLoTD) [20] we proposed recently, the timing noise floor is reduced by more than 5 orders than that of BOC at a 1 mW input power.

Among all the methods mentioned above, balanced photodetection is routinely employed to cancel the laser’s amplitude noise and background environmental noise. Therefore, two photodiodes are inevitably required. However, the conversion from the optical pulse to the electronic pulse typically accompanies a highly nontrivial excess noise (photogenerated carriers, carrier scattering, energy-dependent space charge effects, etc.) in the photodetectors. These uncorrelated electronic noises arising from two independent photodetection processes are difficult to exclude by the balanced subtraction, leading to an imperfect measurement and hampering the resolution at a high-frequency range above 10 kHz. To this matter, a modified BLoTD scheme with only a single photodiode (SP-BLoTD) is proposed and experimentally demonstrated in this work. Using a novel balanced configuration with time and frequency multiplexing, the electronic noise from photodetection can be well suppressed.

The principle of the SP-BLoTD is illustrated in Fig. 1(a). The laser pulse with an optical carrier angular frequency of  $\omega_0$  is divided into two arms. On one arm, a frequency shifter (FS) is applied to yield two isolated pulses with different frequency offsets:  $m\omega_{RF}$  and  $n\omega_{RF}$  ( $m$  and  $n$  are natural numbers), denoted as pulse #1 and pulse #2, respectively. On the other arm, timing shifts  $\Delta t$  are introduced by a timing element, and then the pulse is divided into #a and #b using a time division multiplexing (TDM) element. By carefully tuning the delay in TDM and in the path of pulse #2, the desired delay time among the four pulses is obtained, as shown in Fig. 1(b). The output electric field of the multi-port coupler (MPC) can be written as

$$E(t) = \sum_{k=-\infty}^{+\infty} \begin{bmatrix} A(t - \Delta t - kT)e^{-j\omega_0(t-\Delta t)} \\ + A(t - \Delta t - T_D - kT)e^{-j\omega_0(t-T_D-\Delta t)} \\ + A(t - kT)e^{-j(\omega_0+m\omega_{RF})t} \\ + A(t - \tau_d - T_D - kT)e^{-j(\omega_0+n\omega_{RF})(t-\tau_d-T_D)} \end{bmatrix}, \quad (1)$$

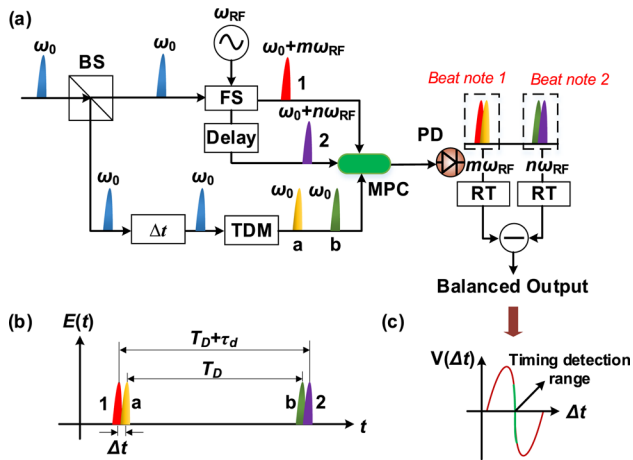


**Fig. 1.** (a) Principle of the SP-BLoTD scheme. BS, beam splitter; FS, frequency shifter;  $\Delta t$ , timing element; TDM, time division multiplexing; MPC, multi-port coupler; PD, photodiode; RT, rectifier. (b) The output pulses of MPC in the time domain. (c) Timing characterization curve.

where  $A(t)$  is the pulse envelope,  $T_D$  is a large delay making sure that during the variation of  $\Delta t$ , pulse #1/2 can only overlap with pulse #a/b, respectively, while  $\tau_d$  is a fine delay to guarantee pulse #2's rising edge overlaps with pulse #b' falling edge, when pulse #1's falling edge overlaps with pulse #a' rising edge.

After passing the PD, two RF beat note signals  $m\omega_{RF}$  and  $n\omega_{RF}$  are generated from the beating of pulse pair 1-a and 2-b, respectively. The timing information  $\Delta t$  encoded in the amplitude fluctuation of the two beat notes can be extracted by rectifiers [20]. Based on Eq. (1), the final output voltage after balanced subtraction is

$$V(\Delta t) \propto \left| \int_{-\infty}^{+\infty} A(t)A(t - \Delta t)^* dt \right|^\alpha - \left| \int_{-\infty}^{+\infty} A(t - \tau_d)A(t - \Delta t)^* dt \right|^\alpha, \quad (2)$$

where  $\alpha$  is a parameter associated with nonlinearities of the rectifier. For typical pulse shapes (Gaussian, hyperbolic secant, etc.), the relation between  $V$  and  $\Delta t$  is an "s" curve (Fig. 1(c)), the slope around the zero-crossing point can be optimized by  $\tau_d$ . Since the two RF beat notes come from the same PD, the common electronic noise during photodetection can be substantially suppressed.

A typical experimental setup for evaluating SP-BLoTD is depicted in Fig. 2(a). A passive mode-locked laser (MENHIR-1550) delivers a hyperbolic secant-shape pulse train centered at 1557.7 nm with a 240 fs duration and 216.667 MHz repetition rate. A polarization beam splitter (PBS) firstly divides the laser into the delay arm and the modulation arm. On the modulation arm, the light passes through a circulator and then launches into a fiber-coupled acousto-optics frequency shifter (AOFS). A function generator (Keysight 33622A) outputs 80 MHz, 200 mVrms sine signal, and is subsequently amplified to 3 W to drive the AOFS. After modulating by the AOFS, the 1st-order diffraction light with 80 MHz carrier frequency shift is generated and transferred into free space. A 70R/30 T beam splitter mounted on a manual stage is used to partially transmit/reflect the 1st-order light. The reflected part goes through the AOFS again, and its carrier frequency is shifted by another 80 MHz to create the 2nd-order diffraction light. The light on the delay arm maintains

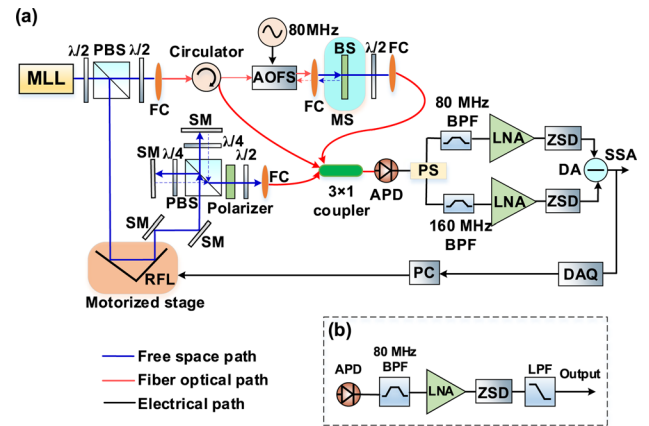


**Fig. 2.** (a) Schematic experimental setup of SP-BLoTD. (b) A single-path measurement setup. MLL, mode-locked laser; FC, fiber collimator; BS, beam splitter; SM, silver mirror;  $\lambda/2$ , half-wave plate;  $\lambda/4$ , quarter wave plate; MS, manual stage; RFL, retroreflector; APD, avalanche photodiode; PS, power splitter; LNA, low-noise amplifier; ZSD, zero-bias Schottky diode; BPF, band-pass filter; LPF, low-pass filter; DA, differential amplifier; DAQ, data acquisition card; PC, personal computer; SSA, signal source analyzer.

the original carrier frequency, denoted as the 0th-order light (not to be confused with the 0th-order AOFS transmission light). A retroreflector sitting on a motorized stage is adopted to introduce timing shifts  $\Delta t$ . A TDM which consists of a PBS, two quarter wave plates, two silver mirrors, and a polarizer is utilized to split the 0th-order light into two pulse trains ( $0^a$  and  $0^b$ ) with a relative delay of  $T_D$ . The zeroth-, 1st-, and 2nd-order light are combined together by a  $3 \times 1$  fiber coupler.

After an avalanche photodiode (APD, CONQUER KG-APR-100M-A-FC), two RF beat notes of 80 MHz ( $0^a$ -1st) and 160 MHz ( $0^b$ -2nd), are obtained. Each beat note signal is band-pass filtered and amplified by a low-noise amplifier (Mini-Circuits, ZX60-P103LN+). To resolve the timing shifts  $\Delta t$ , a zero-bias Schottky diode (ZSD, Connphy Microwave ZBS-0.01-18.5G) is used to extract the power fluctuation of each beat note. Finally, the balanced detection is accomplished with a low-noise differential amplifier ( $\sim 0.75$  nV/ $\sqrt{\text{Hz}}$  input voltage noise and  $\sim 1$  MHz bandwidth).

Polarization-maintaining fiber optics is applied in the whole setup to avoid the polarization mode dispersion effect. The whole setup is covered by a customized enclosure to isolate external perturbations, such as temperature fluctuations, mechanical vibrations, and acoustics noise.

To optimize the timing sensitivity of the SP-BLoTD, output voltages of the two ZSDs are firstly sampled with a data acquisition card while the computer-controlled motorized stage is moving, as shown in Fig. 3(a). Since the 3 dB bandwidth of the APD is only 100 MHz, the 160 MHz beat note is weaker than the 80 MHz one. To ensure the two curves in Fig. 3(a) have almost equal peak amplitudes, a 5 dB attenuator is added after the band-pass filter at the 80 MHz electronic path. The delay  $\tau_d$  is also carefully chosen by adjusting the manual stage. With the two operations above, the two curves can coincide at their maximum slope points, which can provide the maximum timing sensitivity after the balanced subtraction. By collecting the output voltages of the differential amplifier at different motorized stage positions (i.e., different  $\Delta t$ ), the timing characterization curves are

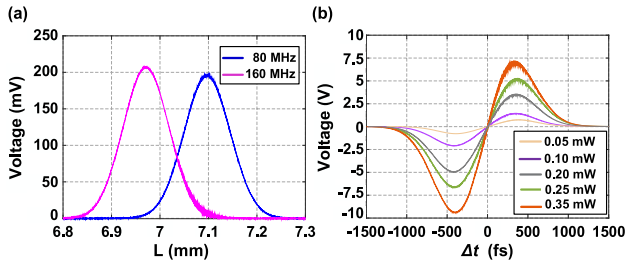


**Fig. 3.** (a) The output voltages of the two ZSDs at different motorized stage positions. (b) Timing characterization curves with different input optical powers per pulse train.

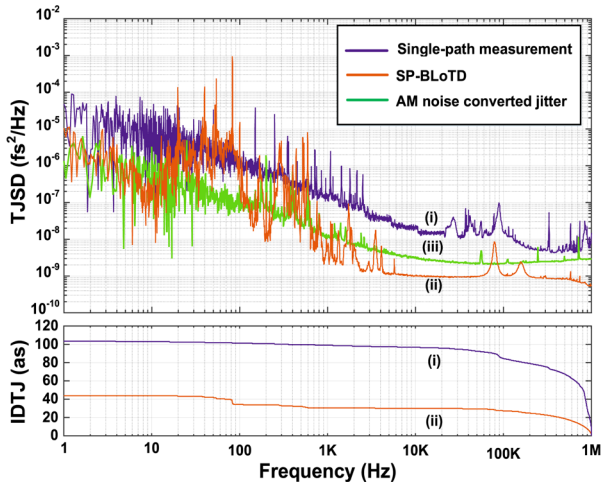


**Fig. 4.** Measurement results: the timing jitter spectral density (up) and the corresponding integrated timing jitter (down). Input power of APD: 0.35 mW per pulse train.

obtained (Fig. 3(b)). With a total input optical power of 1.4 mW (0.35 mW for 0<sup>a</sup>, 0<sup>b</sup>, 1st, and 2nd pulse trains, respectively) before the APD, the timing sensitivity around the zero-crossing point is about 34.60 mV/fs (Fig. 3(b), brown curve). In Fig. 3(b), the zero-crossing points of all timing curves with different input optical powers perfectly coincide, indicating that the SP-BLoTD is insensitive to the laser's power fluctuation.

In order to investigate the detection limit of the SP-BLoTD, the baseband noise outputs from the differential amplifier is measured by a signal source analyzer (SSA, Holzworth HA7062C) around the zero-crossing position in Fig. 3(b). With an APD input power of 0.35 mW per pulse train, the measured timing jitter spectral density (TJSD) is shown in the upper part of Fig. 4 (curve (ii)). For comparison, a single-path measurement, which replaces the balanced electronics after APD with the setup in Fig. 2(b), is executed. The corresponding TJSD is presented as curve (i) in the upper part of Fig. 4. Besides, the amplitude noise of the 80 MHz beat note from the output port in Fig. 2(b) (which includes the amplitude fluctuation of both the laser and the RF driving signal imposed on the AOFS) is also measured by the SSA and converted to the timing jitter (Fig. 4, curve (iii)). It should be noted that multiple spikes and bumps from 20 kHz to 1 MHz appear in curve (i) but not in curve (ii) and curve (iii), which prove that they are electronic noises aroused from the APD photodetection process rather than the laser source. The dominant APD electronic noise as well as the laser and

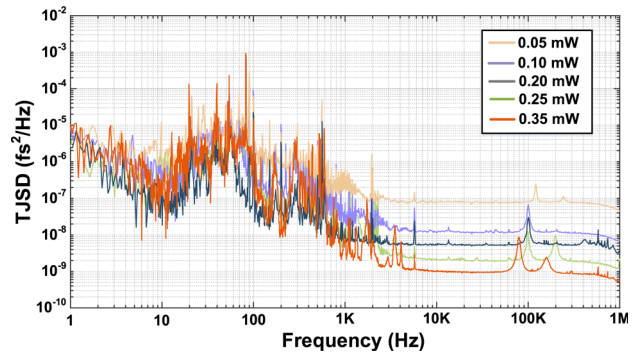


**Fig. 5.** Measured TJSD at different input powers per pulse train of APD.

RF amplitude noise is significantly suppressed after balanced detection, resulting in an exceptionally low timing noise floor of approximately  $8 \times 10^{-10}$  fs<sup>2</sup>/Hz (Fig. 4, curve (ii)), which is almost shot noise limited based on theoretical calculation [20]. Ranging from 10 kHz to 1 MHz, the TJSD of the SP-BLoTD is almost flat except for two residual peaks around 100–200 kHz. These perfect eliminations of the photodetector electronic noise are impossible for our previous scheme [20], as well as any other balanced timing detectors using two independent photodiodes.

The integrated timing jitter (IDTJ) for SP-BLoTD and the single-path measurement are given at the bottom of Fig. 4. Due to the APD electronic noise suppression, the IDTJ at [1 kHz and 1 MHz] is reduced from 99.0 as in the single-path measurement to 30.4 as in SP-BLoTD. Finally, the SP-BLoTD exhibits a total integrated timing jitter of approximately 43.73 as over the frequency range of 1 Hz to 1 MHz, which corresponds to a detection dynamic range of 84.69 dB within the monotone interval of the timing characterization curve ( $\sim 750$  fs in Fig. 3(b)).

We also carried out several measurements with different input optical power levels to fully exploit the high resolution of SP-BLoTD. By decreasing the injected optical power per pulse train at APD from 0.35 to 0.05 mW, the corresponding TJSD is given in Fig. 5. With the decrease of the input power, the noise floor continuously raises due to the increase of the shot-noise-limited timing jitter. For all cases, the flat noise floor above 10 kHz indicates that SP-BLoTD can always eliminate the photodetector electronic noise at the milliwatt to microwatt input power levels. With 0.05 mW per pulse train, the timing detection floor is 221.4 zs/ $\sqrt{\text{Hz}}$  and the IDTJ from 1 kHz to 1 MHz is only 268.0 as. This impressive attosecond precision at the microwatt power level makes SP-BLoTD a good candidate for ultra-long-distance ranging and timing synchronization [21].

The timing detection floor for BLoTD and SP-BLoTD at extremely low-power levels are calculated and compared in Table 1. Since the electronic-noise-converted timing jitter would be more serious (if were not suppressed) at lower input power levels, the advantage of SP-BLoTD over BLoTD becomes more and more significant as the power decreases.

In conclusion, we have demonstrated an attosecond-resolution timing detector SP-BLoTD based on a double-pass fiber-coupled acousto-optics frequency shifter. Using a novel time and frequency multiplexing configuration, balanced timing detection is realized with only a single photodiode for the first time to our knowledge. The excess electronic noise during photodetection is well suppressed. With a photodiode input optical power of 0.35 mW per pulse train, the timing detector exhibits a noise

**Table 1. Calculated Timing Detection Floor for BLoTD and SP-BLoTD at Different Inject Optical Powers of APD**

Optical Power per Pulse Train ( $\mu\text{W}$ )	BLoTD (as/ $\sqrt{\text{Hz}}$ )	SP-BLoTD (as/ $\sqrt{\text{Hz}}$ )
20	0.522	0.429
10	0.861	0.623
5	1.505	0.925
1	6.534	2.722
0.1	62.887	20.661

floor of  $8 \times 10^{-10}$  fs<sup>2</sup>/Hz and 84.69 dB dynamic range. Even the input power is reduced to 50  $\mu\text{W}$  per pulse train, attosecond precision is still maintained with 268.0 as IDTJ at [1 kHz and 1 MHz]. With a higher saturation power photodetector, it is possible to push the timing resolution of SP-BLoTD to the zs level. Due to the simplicity of the structure, a fully-on-chip SP-BLoTD could be realized [22,23] to unlock portable applications. Utilizing its excellent performance at the  $\mu\text{W}$  level, SP-BLoTD will also provide great prospects for various scenarios in remote optical frequency synthesis [24,25], space gravitational wave detection [26], and quantum-limited ranging [27].

**Funding.** National Key Research and Development Program of China (2021YFC2201902); National Natural Science Foundation of China (61975149).

**Disclosures.** The authors declare no conflicts of interest.

**Data availability.** Data underlying the results presented in this paper are not publicly available at this time but may be obtained from the authors upon reasonable request.

## REFERENCES

- M. Xin, K. Şafak, and M. Y. Peng, *et al.*, *Opt. Express* **22**, 14904 (2014).
- M. Xin, K. Şafak, and M. Y. Peng, *et al.*, *Light: Sci. Appl.* **6**, e16187 (2016).
- K. Şafak, M. Xin, and M. Y. Peng, *et al.*, *Sci. Rep.* **8**, 11948 (2018).
- M. Harmand, R. Coffee, and M. R. Bionta, *et al.*, *Nat. Photonics* **7**, 215 (2013).
- H. W. Kim, N. A. Vinokurov, and I. H. Baek, *et al.*, *Nat. Photonics* **14**, 245 (2020).
- J. Stohr, "Linac coherent light source II (LCLS-II) conceptual design report," Design Report SLAC-R-978 (SLAC, 2011).
- Z. Zhao, D. Wang, and Q. Gu, *et al.*, *Synchrotron Radiation News* **30**, 29 (2017).
- X. Lu, S. Zhang, and X. Chen, *et al.*, *Sci. Rep.* **7**, 13305 (2017).
- H. Bergeron, L. C. Sinclair, and W. C. Swann, *et al.*, *Nat. Commun.* **10**, 1819 (2019).
- G. M. Rossi, R. E. Mainz, and Y. Yang, *et al.*, *Nat. Photonics* **14**, 629 (2020).
- Y. He, K. G. H. Baldwin, and B. J. Orr, *et al.*, *Optica* **5**, 138 (2018).
- Y. Na, C.-G. Jeon, and C. Ahn, *et al.*, *Nat. Photonics* **14**, 355 (2020).
- Y. Na, H. Kwak, and C. Ahn, *et al.*, *Light: Sci. Appl.* **12**, 44 (2023).
- Y. Song, F. Zhou, and H. Tian, *et al.*, *Optica* **7**, 1531 (2020).
- D. Zou, Y. Song, and O. Gat, *et al.*, *Optica* **9**, 1307 (2022).
- T. R. Schibli, J. Kim, and O. Kuzucu, *et al.*, *Opt. Lett.* **28**, 947 (2003).
- A. Casanova, A. Courjaud, and B. Tropheime, *et al.*, *Opt. Lett.* **45**, 6098 (2020).
- D. Hou, C.-C. Lee, and Z. Yang, *et al.*, *Opt. Lett.* **40**, 2985 (2015).
- D. Kwon, C. Jeon, and J. Shin, *et al.*, *Sci. Rep.* **7**, 40917 (2017).
- T. Wang, Q. Ren, and K. Şafak, *et al.*, *Opt. Express* **29**, 38140 (2021).
- M. Xin, K. Şafak, and F. X. Kärtner, *Optica* **5**, 1564 (2018).
- E. A. Kittlaus, W. M. Jones, and P. T. Rakich, *et al.*, *Nat. Photonics* **15**, 43 (2021).
- Y. Hu, M. Yu, and D. Zhu, *et al.*, *Nature* **599**, 587 (2021).
- M. Xin, N. Li, and N. Singh, *et al.*, *Light: Sci. Appl.* **8**, 122 (2019).
- N. Singh, M. Xin, and N. Li, *et al.*, *Laser Photonics Rev.* **14**, 1900449 (2020).
- P. A. Seoane, S. Aoudia, and S. Babak, *et al.*, *Class. Quantum Grav.* **29**, 124016 (2012).
- E. D. Caldwell, L. C. Sinclair, and N. R. Newbury, *et al.*, *Nature* **610**, 667 (2022).